ACS OMEGA

http://pubs.acs.org/journal/acsodf

Article

Low-Temperature Operating Black SnO_2-Based VOC Sensor Setup

Kiran Mahalingappa, Gowtham Maralur Pranesh, Gopinatha Bidarkatte Manjunath, Shridhar Mundinamani,* Shilpa Molakkalu Padre, Nirankar Nath Mishra, and Gurumurthy Sangam Chandrasekhar*

Cite This: *ACS Omega* 2021, 6, 22900−22908

Read Online

ACCESS | Metrics & More | Article Recommendations | Supporting Information

ABSTRACT: Volatile organic compounds (VOCs) are harmful to human beings and animals. VOCs include a carbon compound and its derivatives. VOCs irritate the eyes, ears, and throat, ahigh concentration of VOCs may cause cancer; also, it affects the central nervous system. A concentration below 0.3 mg/m^3 is harmless, above which it is harmful to human beings. The present work discusses the detection of harmful VOCs using a lab-made portable device setup. Hydrothermally synthesized tin oxide (SnO_2) nanocubes are used as an active material for VOC detection. The SnO_2 pellet is prepared using a hydraulic press method and is used in the portable setup. Temperature-dependent VOC detection is carried out using a microheater. An external potential is applied to the microheater, which stimulates the active material to sense ethanol at 40 °C. SnO_2 and EA deposited on graphite interdigitated electrodes projected on cellulose are used to detect isopropanol, ethanol, and acetone at room temperature. Temperature-dependent studies on acetone are carried out. A significant change in the current levels is observed for different VOCs. A positive shift in the Dirac point is noticed upon VOC exposure. The developed portable device plays a vital role in analyzing sensors based on various active materials for VOC detection.

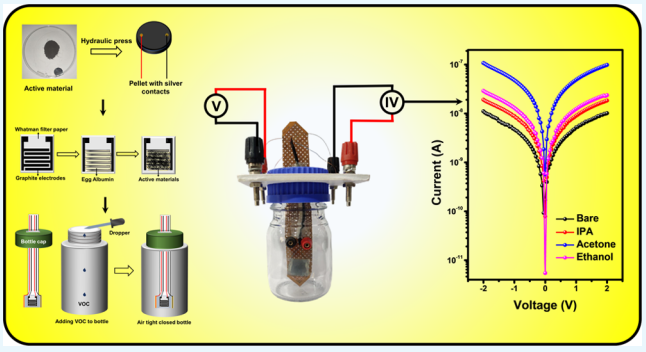

INTRODUCTION

Some hydrocarbon-based volatile compounds are harmful to humans, aquatic life, plants, and the environment.[1] High concentration of combustible organic compound-based gases (volatile organic compounds (VOCs)) and more exposure to VOC irritate eyes, ears,[2] and skin; hence, adsorption,[3] detection, and monitoring of these VOCs are essential. For the detection of VOCs, a paper-based three-layered sensing milli-cantilever is used. A change in the position of the cantilever indicates the presence of VOCs.[4,5]

Palladium-doped ZnO nanorods are used to detect VOCs at room temperature;[6] in this sensor, the heavy metal Pd is used as an active material, which upon disposal affects the ecosystem. A three-dimensional nanostructured architecture comprising graphene oxide/ZnO heterojunctions has been used to sense the volatile biomarker at room temperature.[7] Co_3O_4 nanorods prepared by a hydrothermal method are used as the active material for the detection of VOCs like benzene, acetone, and ethanol at different temperatures,[8] and ethanol is detected using silver-doped TiO_2/SnO_2 nanocomposites at higher temperatures.[2] A ruthenium-based complex deposited on aluminum interdigitated electrodes is used for VOC sensing applications.[9]

In the last few decades, research work is carried out on the detection and monitoring of VOCs by various sophisticated instruments that are not economical and portable. The present work emphasizes the design and fabrication of a low-cost, portable device setup for the detection of VOCs. The device setup is tested using a black SnO_2 pellet for the detection of ethanol at 40 °C and a composition of black SnO_2 and egg albumin (EA) deposited onto the cellulose and pencil (graphite)-based interdigitated electrodes and SnO_2 pellet as an active material for the detection of isopropyl alcohol, ethanol, and acetone at room temperature and higher temperatures.[10]

RESULTS AND DISCUSSION

Detection of Ethanol Using the SnO_2 Pellet. The prepared SnO_2 pellet acts as a sensing material and is connected to the bottle setup, and the bottle is made airtight. The IV characterization is carried out for bare SnO_2 without any VOC and in the presence of 4 μL of ethanol in the bottle setup.

Received: July 1, 2021
Accepted: August 4, 2021
Published: August 26, 2021

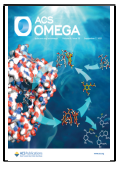

https://doi.org/10.1021/acsomega.1c03399
ACS Omega 2021, 6, 22900−22908

Detection of IPA, Ethanol, and Acetone Using IDE. The dried SnO_2/ EA-deposited IDE (S-IDE) is connected to the bottle setup using connecting wires. The IV characterizations are performed for bare S-IDE and with concentrations of IPA, ethanol, and acetone of 8 ppb each, whereas the permissible exposure limit to these VOCs is 0.5 ppm. The present sensor works in the range of 8 ppb to 32 ppm for all of these VOCs. Here, the sensing mechanism is based on adsorption of VOCs onto the active material. Upon obtaining the data, the bottle setup is washed completely and dried to remove the residues of measured VOC and used for the next VOC measurement. The same steps are repeated for the individual VOC measurements.

Temperature Dependence Study Using Acetone. The temperature dependence study is carried out using a specified volume of acetone, i.e., 4 μL of acetone is added to the bottle, and the microheater is provided with the required DC voltage. The response of the sensor to the same VOC, i.e., acetone, is recorded at a different level of temperature. Addition of VOCs is shown in Figure 1.

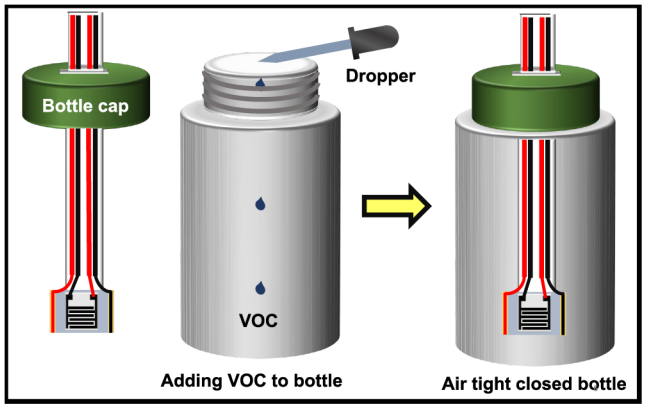

Figure 1. Schematic representation of adding VOCs to the portable device setup.

Figure 2 shows the SEM images of synthesized black SnO_2 under different resolutions. Figure 2a shows a highly porous surface and reveals the cuboid morphology of black SnO_2. Figure 2b of a higher magnification confirms the formation of micron-sized cuboids. An enlarged cuboid image of black SnO_2 is shown in Figure 2c. Further, the formation of black SnO_2 is confirmed by EDX analysis, as shown in Figure 2d The oxygen peak is observed at 0 keV, and Sn peaks were observed at 3.45 and 3.67 keV.

The crystalline structure of the black SnO_2 cuboids analyzed by XRD is shown in Figure 2e. The diffraction patterns of synthesized black SnO_2 indicated a tetragonal cassiterite structure of SnO_2. As per JCPDS no. 41-1445, the observed peaks at 2θ = 26.6, 33.8, 38.1, 51.8, 54.7, 61.9, 65.9, and 66.0 are indexed to the (110), (101), (200), (211), (220), (310), and (301) planes of the SnO_2 phase, respectively. The estimated particle size by the Debye−Scherer formula is 18 nm.

The digital photographs of the glass bottle setup are shown in Figure 3a−c. Figure 3a shows the front view of the bottle setup. Figure 3b shows a front view of a bottle cap along with a microheater and a sensor holder. Figure 3c shows the top view of a bottle cap seen with connecting wires for the sensor and microheater.

The schematic representation of the setup using the SnO_2 pellet is shown in Figure 4. The interdigitated electrodes are prepared using graphite. The deposition of graphite is carried out by writing mechanically in the form of IDEs on the Whatman filter paper substrate. The IDEs are overwritten seven times repeatedly to achieve a uniform sheet resistance. The end-to-end resistance of each finger electrode is 1 kΩ. Further, EA (20 mg in 5 mL of DI water) is deposited by drop-casting on the surface of prepared IDEs and dried under a lamp for 1 h. One gram of black SnO_2 is mixed with 10 mL of DI water and ground for 20 min in a pestle mortar. The black SnO_2 solution is drop-casted on EA-deposited IDEs. The schematic representation of the preparation of EA and SnO_2

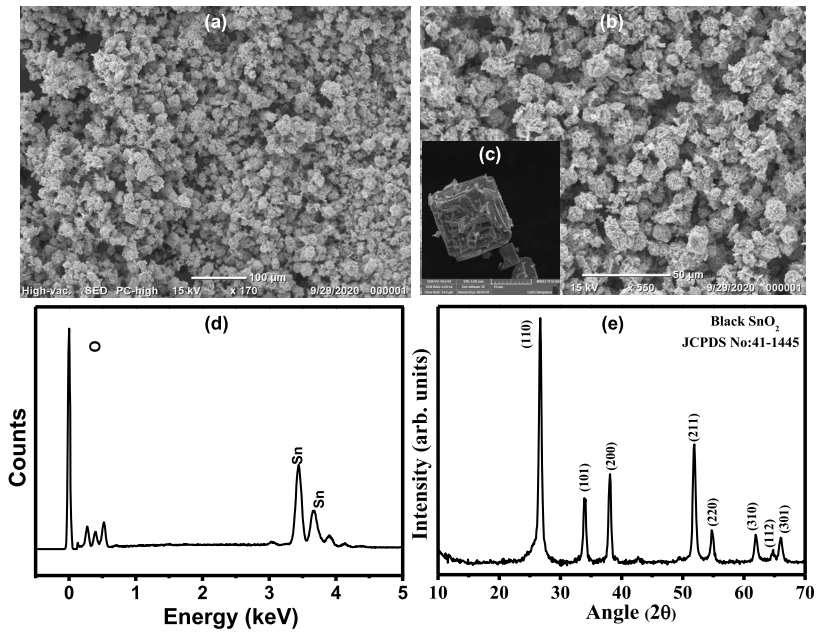

Figure 2. Scanning electron microscopy images of (a) black SnO_2, (b) black SnO_2 at higher magnification, and (c) black SnO_2 at still higher magnification; (d) energy-dispersive X-ray graph of black SnO_2; and (e) X-ray diffraction pattern of black SnO_2.

https://doi.org/10.1021/acsomega.1c03399
ACS Omega 2021, 6, 22900−22908

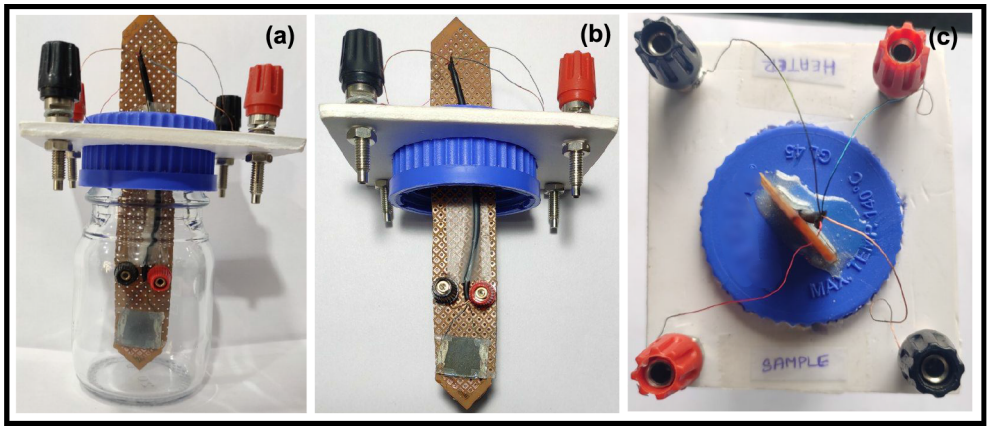

Figure 3. Optical photographs of the portable bottle setup: (a) front view, (b) front view of the opened portable bottle setup, and (c) top view of the portable bottle setup.

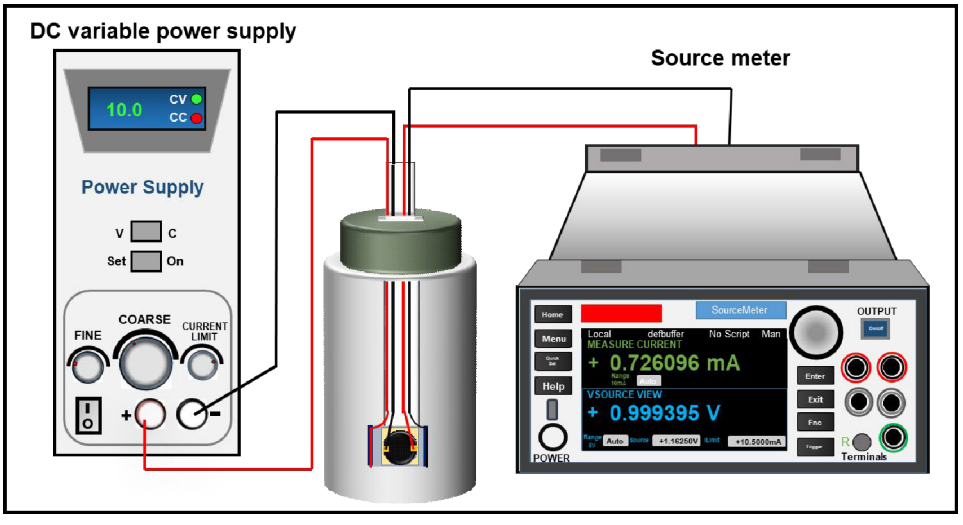

Figure 4. Schematic representation of the connection of the portable bottle setup with the heater and source meter for $I-V$ characterization.

deposition on IDEs is shown in Figure 5. Further, the prepared IDEs are used for current−voltage characterization. The

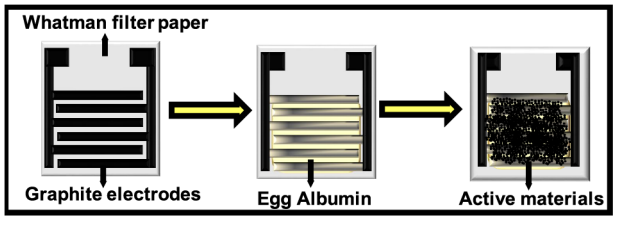

Figure 5. Schematic representation of fabrication of S-IDE.

schematic representation of the SnO_2 IDEs for current−voltage measurements is similar to that in Figure 4.

VOC Sensing Properties. Commercially available gas sensing setups are not economical. Hence, the proposed method will be very much useful for VOC detection. First, the synthesized black SnO_2 pellet is used, $I-V$ curves are recorded, and the logarithmic current−voltage is plotted in a potential window of ±2 V at 300 K, as shown in Figure 6a. As evidenced from the $I-V$ curves, black SnO_2 (black curve) shows low conductivity for an applied voltage of 2 V, and the observed current is 5.96 nA. The curve is symmetric in both reverse and

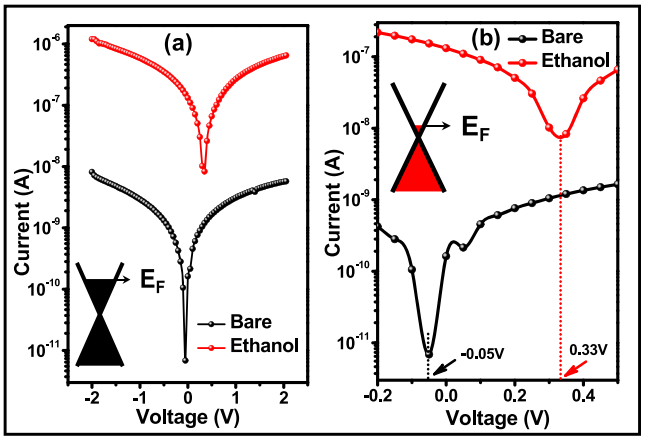

Figure 6. Current−voltage characteristics of (a) bare black SnO_2 (black line) and under ethanol vapor exposure (red line) at 315 K with ±2 V potential window (the inset shows the schematic representation of the Fermi level (E_F)). (b) Enlarged current−voltage characteristics of bare black SnO_2 (black line) (the Dirac point is 0.05 V) and under ethanol vapor exposure (red line) (the Dirac point is 0.33 V) at 315 K in the −0.2 to 0.5 V range (the inset shows the schematic representation of the Fermi level (E_F)).

https://doi.org/10.1021/acsomega.1c03399
ACS Omega 2021, 6, 22900−22908

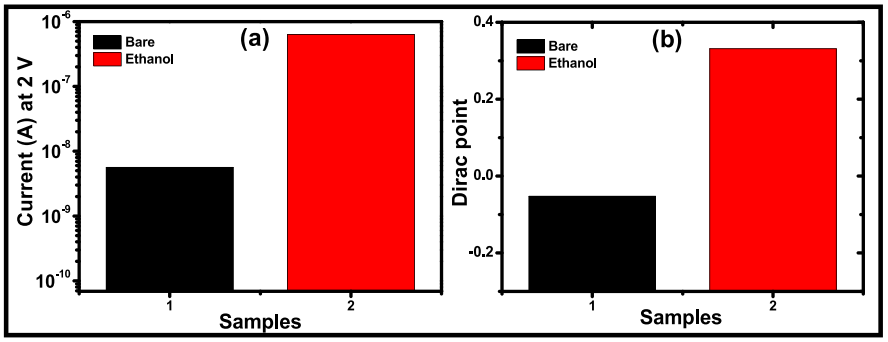

Figure 7. (a) Increment in the current level at 2 V of bare black SnO_2 (black bar) and under ethanol vapor exposure (red bar) at 315 K. (b) Dirac points of bare black SnO_2 (black bar) and ethanol vapor exposure (red bar) at 315 K.

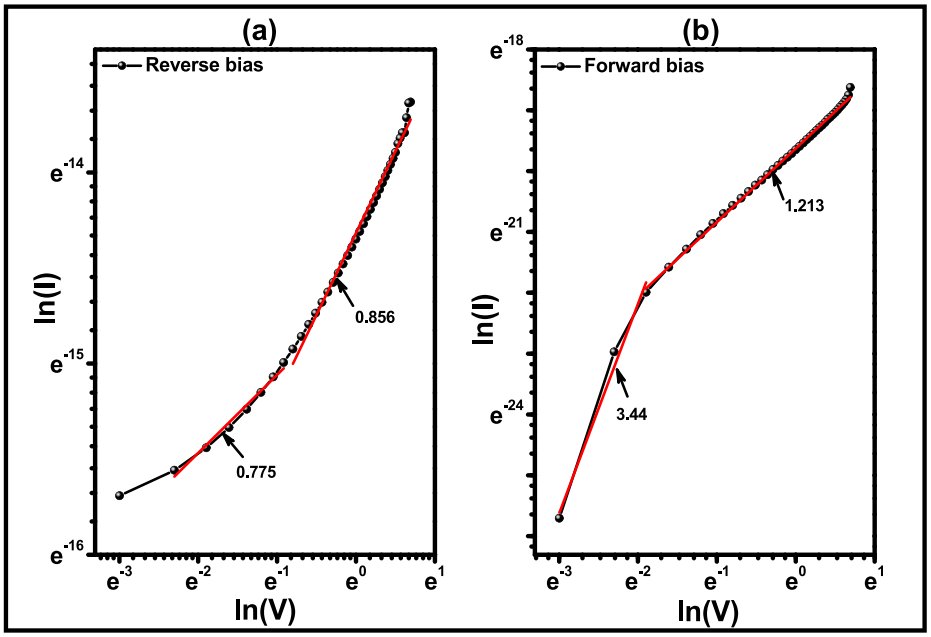

Figure 8. Current−voltage characteristics of bare black SnO_2 under ethanol vapor exposure: (a) reverse bias [ln (I) vs ln (V)] and (b) forward bias [ln (I) vs ln (V)].

forward bias regions, indicating an Ohmic charge transport mechanism. At 300 K, there is no significant increase in the current observed upon ethanol vapor exposure.[11,12] When the temperature of the heater is increased to 315 K, no significant increase in the current is observed for bare SnO_2, and in the presence of ethanol vapors, a 2 order increment in the current is observed. As evidenced from the $I-V$ curves, black SnO_2 (black curve) shows an increment in conductivity for an applied voltage of 2 V, and the observed current is 0.65 μA. In semiconducting materials wherein the conduction band and valence band meet at a single point, the Fermi level at the K point is known as the Dirac point.[13] This Dirac point enables both electrons and holes to transport and hence contributes to diffusion. Because of the band structure of semiconductors, a few devices like FETs show an ambipolar property (the current level is the same both in forward and reverse bias regimes). In the present study, a positive shift in the Dirac point (−0.05 to 0.33 V) is observed when the device is exposed to ethanol vapors. The enlarged curves for Dirac points are shown in Figure 6b. The inset shows the Fermi level of the device when it is exposed to ethanol vapors. This behavior of SnO_2 is usually caused by adsorbed oxygen or water. When SnO_2 is exposed to ethanol vapors at 315 K, the Dirac point is shifted from −0.05 to 0.33 V, indicating a p-type doping effect.[11] This is because of net hole transfer from ethanol to SnO_2 due to cleaning of the surface of SnO_2 by adsorbing the H^+ group of ethanol onto the SnO_2 surface. So, the Fermi energy of SnO_2 is changed, as displayed by the scheme in the inset of Figure 6b. The current increment order confirms the functionalization of SnO_2 in the presence of ethanol vapors, which is occurred by noncovalent bonding. Many researchers have studied the doping of SnO_2 to control its electrical properties and tune its energy level for electronic device applications, such as sensors, photodetectors, and transistors. As per the literature, undoped SnO_2 is found to be a poor conductor of electricity as it forms Schottky contacts with the metal electrode, whereas the doped SnO_2 shows excellent electrical properties.

In Figure 7a, the increment of current values is shown with a bar graph; the black bar is for the pure black SnO_2 device, and the red bar is for ethanol exposure. Similarly, in Figure 7b, the Dirac point values are shown with a bar graph. The black bar is for the pure black SnO_2 device, and the red bar is for the device under ethanol vapor exposure. Upon ethanol exposure, substitutional doping of functional groups to the black SnO_2 material increases the mobility and conductivity of SnO_2

https://doi.org/10.1021/acsomega.1c03399
ACS Omega 2021, 6, 22900−22908

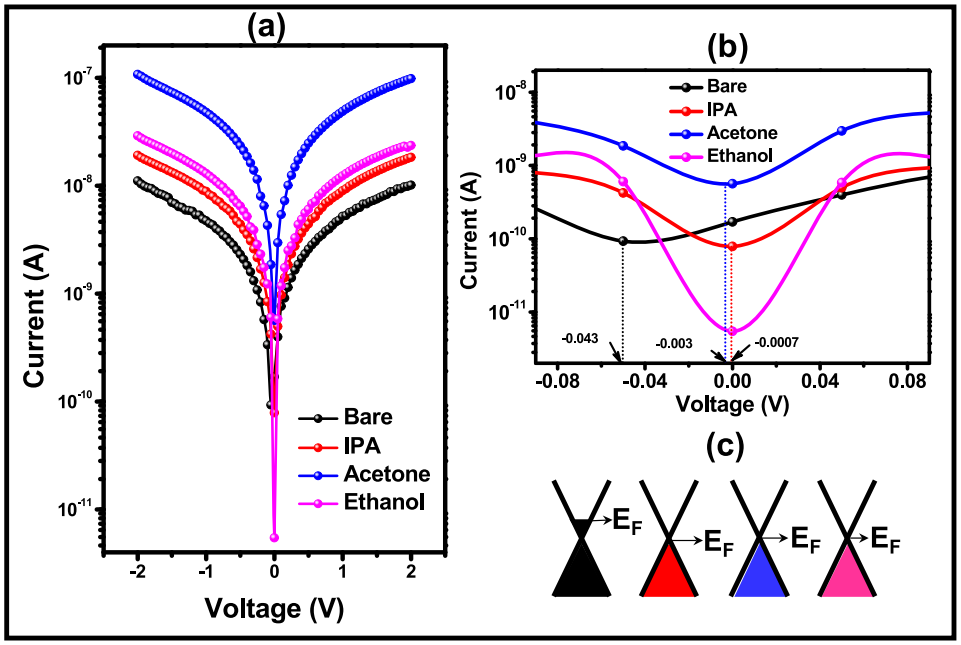

Figure 9. Current−voltage characteristics of S-IDE with a ±2 V potential window at 300 K: (a) bare S-IDE and under IPA, acetone, and ethanol exposure. (b) Enhanced current−voltage characteristics in the range −0.08 to 0.08 V of bare S-IDE (the Dirac point is 0.05 V) and under IPA (the Dirac point is 0.007 V), acetone (the Dirac point is 0.003 V), and ethanol (the Dirac point is 0.007 V) exposure. (c) Schematic representation of Fermi level (E_F) variations with Dirac point shifts under IPA, acetone, and ethanol exposure.

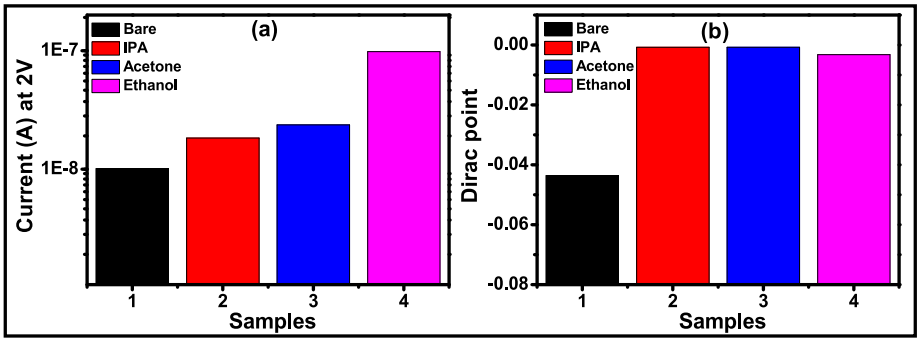

Figure 10. (a) Increment in the current level at 2 V of bare S-IDE (black bar) and under IPA (red bar), acetone (blue bar), and ethanol (pink bar) exposure at 300 K. (b) Dirac points of bare S-IDE (black bar) and under IPA (red bar), acetone (blue bar), and ethanol (pink bar) exposure at 300 K.

because it introduces a considerable number of defects in SnO_2.

Detailed information about the transport mechanism through the SnO_2 pellet can be obtained from the analysis of reverse and forward current−voltage (I−V) characteristics. The reverse and forward bias current−voltage (I−V) characteristics of a SnO_2 pellet are shown in Figure 8a,b. In reverse bias (Figure 8a), at low voltages, the slope of ln (I) vs ln (V) is 0.775, and at higher voltages, the slope is 0.856. These values of slopes indicate an Ohmic region due to thermally generated carriers at lower and higher voltages that are typically an Ohmic conduction mechanism. In forward bias (Figure 8b), at low voltages, the slope of ln (I) vs ln (V) is 3.44, and at higher voltages, the slope is 1.213. These values of slopes indicate the Ohmic region due to thermally generated carriers at the higher and power-law region at lower applied voltages that is typical of a space-charge-limited conduction (SCLC) mechanism controlled by the presence of traps distributed exponentially with energy within the band gap of SnO_2.

Black SnO_2-based device fabrication is carried out using graphite interdigitated electrodes on cellulose paper. Also, this technique helps to make the device portable and flexible. Black SnO_2-deposited cellulose and pencil-based IDE (S-IDE) is used for VOC detection at 300 K, and I−V data are documented. The logarithmic current−voltage is plotted in a potential window of ±2 V at 300 K, as shown in Figure 9a. As evidenced by the logarithmic current−voltage, the S-IDE (black curve) shows low current for an applied voltage of 2 V, and the observed current is 10 nA. The curve confirms the Ohmic charge transport mechanism because of the symmetric behavior in reverse and forward bias regions. S-IDE shows a significant increase in the current level upon the exposure of VOCs like ethanol, IPA, and acetone at room temperature. The addition of 4 μL of IPA to the bottle setup enhances the current level from 10 to 18 nA, as represented in Figure 9a, red line.

Similarly, pink and blue lines represent the I−V curves of 4 μL of ethanol and acetone, respectively. The observed current levels for ethanol and acetone are 23 and 98 nA, respectively,

https://doi.org/10.1021/acsomega.1c03399
ACS Omega 2021, 6, 22900−22908

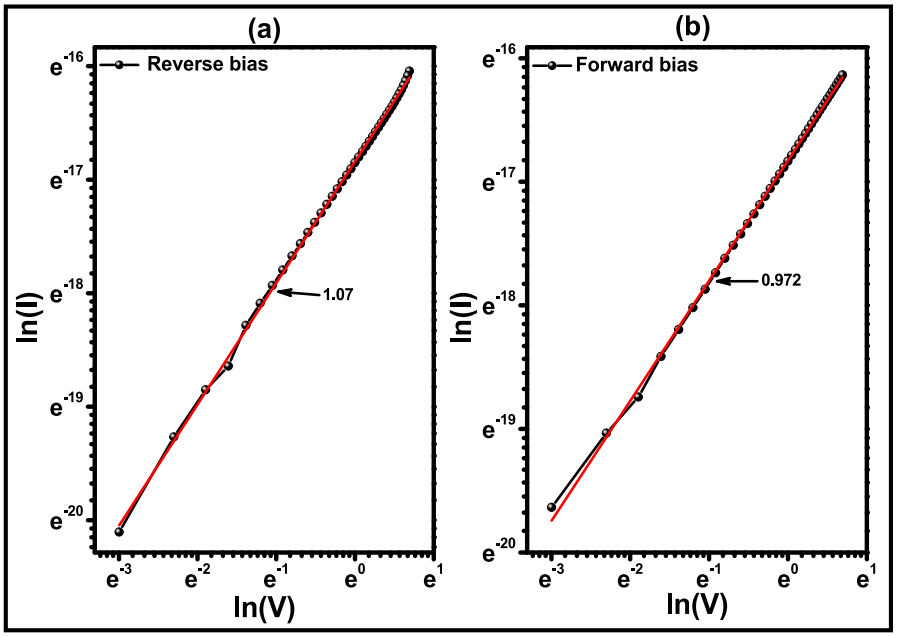

Figure 11. Current−voltage characteristics of bare S-IDE under acetone vapor exposure: (a) reverse bias [ln (I) vs ln (V)] and (b) forward bias [ln (I) vs ln (V)].

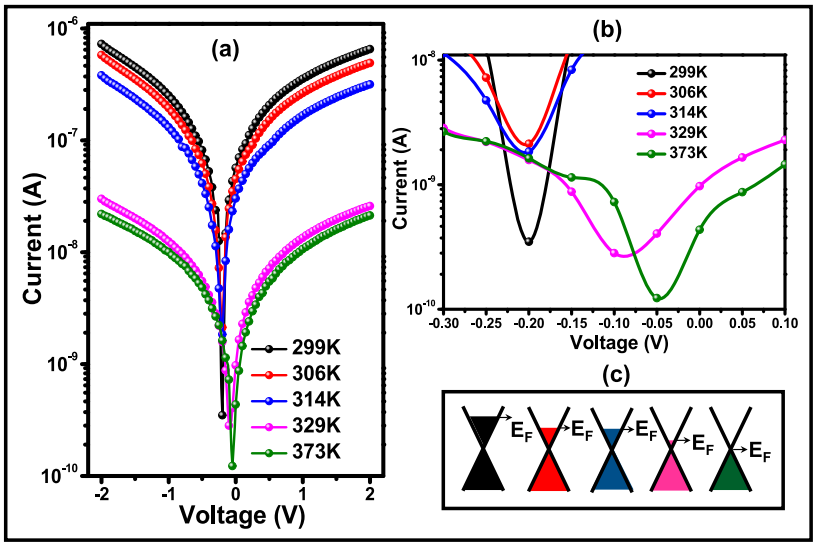

Figure 12. Current−voltage characteristics of S-IDE in the range of ±2 V potential window: (a) acetone exposure at different temperatures. (b) Enlarged current−voltage characteristics in the range −0.3 to 0.1 V and shift of the Dirac point under acetone exposure at different temperatures. (c) Variation in the Fermi level (E_F) with the Dirac point upon the exposure of acetone.

at 2 V. This is in line with the expected charge exchange on the SnO_2 nanomaterial surface, where oxidant species would increase the concentration of free carriers in the metal oxide. Further, the Dirac point shift is investigated for the VOCs, as shown in Figure 9b. The Dirac point shift is observed from −0.04 V (bare SnO_2) to −0.0007 V (IPA), −0.003 V (acetone), and −0.0007 V (ethanol), indicating further p-type doping on the surface of metal oxide. The variation in the Fermi level (E_F) with the Dirac point shift upon VOCs' exposure is shown schematically in Figure 9c.

In Figure 10a, the increment in the current is shown with the bar graph for different VOCs; the black bar is for S-IDE, the red bar is for IPA exposure, the pink bar represents ethanol exposure, and the blue bar is for acetone exposure. Similarly, in Figure 10b, increased Dirac point values upon exposure of VOCs to S-IDE are shown with a bar graph.

Detailed information about the transport mechanism through the S-IDE can be obtained from the analysis of reverse and forward current−voltage (I−V) characteristics. The reverse and forward bias current−voltage (I−V) characteristics of S-IDE are shown in Figure 11a,b. In reverse bias (Figure 11a), at low voltages and high voltages, the slope of ln (I) vs ln (V) is 1.07. The value of slope indicates the Ohmic region due to thermally generated carriers at lower and higher voltages that are typically an Ohmic conduction mechanism. In forward bias (Figure 11b), at low voltages and high voltages, the slope of ln (I) vs ln (V) is 0.972. The value of slope indicates an Ohmic region due to thermally generated carriers.

https://doi.org/10.1021/acsomega.1c03399
ACS Omega 2021, 6, 22900−22908

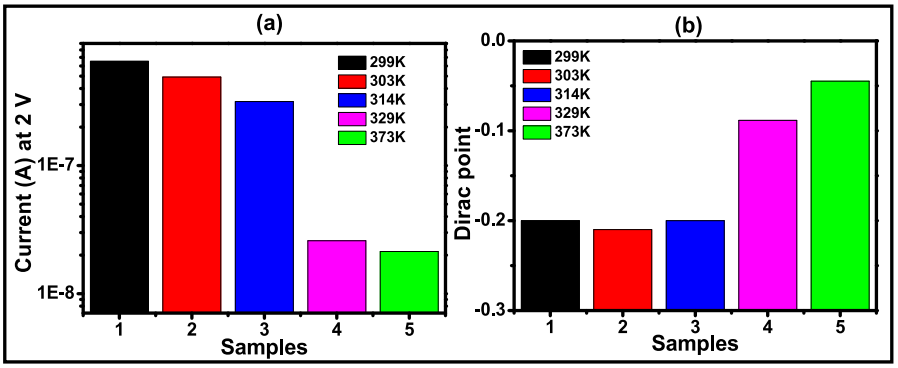

Figure 13. (a) Increment in the current level at 2 V of bare S-IDE (black bar) and under acetone exposure at different temperatures. (b) Dirac points of bare S-IDE (black bar) and under acetone exposure at different temperatures.

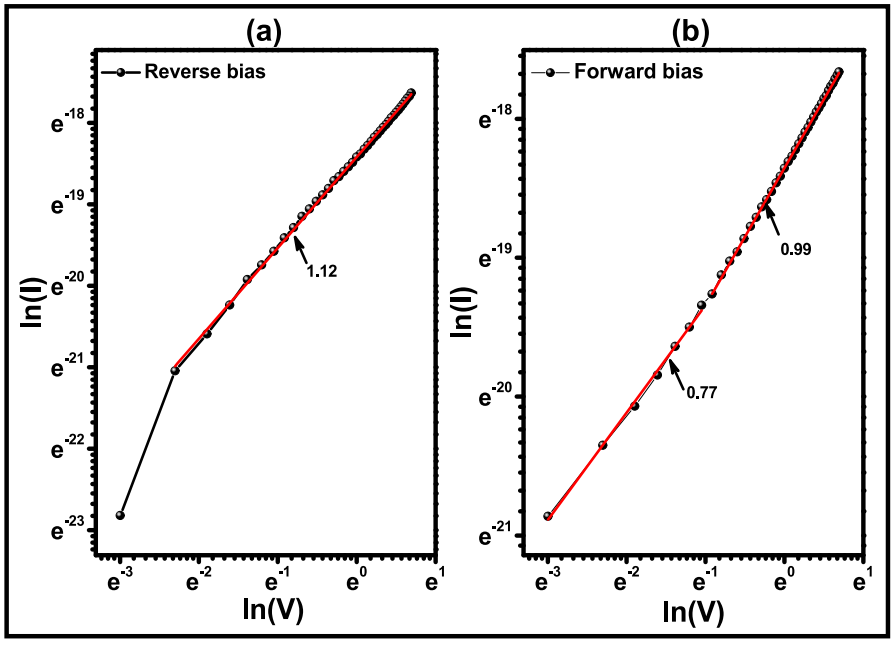

Figure 14. Current−voltage characteristics of bare S-IDE under acetone vapor exposure at 373 K: (a) reverse bias [ln (*I*) vs ln (*V*)] and (b) forward bias [ln (*I*) vs ln (*V*)].

S-IDE's response toward acetone vapors is high, and hence, the temperature-dependent studies are performed. The *I*−*V* curve w.r.t. temperature is shown in Figure 12a. The temperature is varied by applying a constant voltage to the transparent microheater used in the bottle setup. The measurements were carried out after 3 min until the heater reaches a saturation level. The black curve represents the *I*−*V* curve at 299 K (0 V); similarly, red, blue, pink, and green show the *I*−*V* curves at 306 K (5 V), 314 K (10 V), 329 K (15 V), and 373 K (20 V), respectively; as the temperature increases, the mobility and conductivity of the SnO_2 material decrease due to the temperature effect, which creates more surface defects and hinders electronic diffusion. The enlarged Dirac point shift in the *I*−*V* curve is plotted in Figure 12b. A positive shift in the Dirac point is observed with increasing temperature. Dirac points are at −0.21 V for 299 K, −0.2 V for 306 K, 0.2 V for 314 K, −0.089 V for 329 K, and −0.045 V for 373 K. The shift in the Fermi level w.r.t. temperature under acetone vapor exposure is shown schematically in Figure 12c.

In Figure 13a, Dirac point values are shown with a bar graph. The change in the current level under acetone vapors at different temperatures is represented with a bar graph depicted in Figure 13b. Detailed information about the transport mechanism through the S-IDE w.r.t. increasing temperature can be obtained from the analysis of reverse and forward current−voltage (*I*−*V*) characteristics at high temperatures (373 K). The reverse and forward bias current−voltage (*I*−*V*) characteristics are shown in Figure 14a,b. In reverse bias (Figure 14a), at low voltages and high voltages, the slope of ln (*I*) vs ln (*V*) is 1.12. The slope's value indicates the Ohmic region due to thermally generated carriers at lower and higher voltages that are typically an Ohmic conduction mechanism. In forward bias (Figure 14b), at low voltages and high voltages, the slopes of ln (*I*) vs ln (*V*) are 0.77 and 0.972, respectively. The value of the slope indicates an Ohmic region due to thermally generated carriers.

CONCLUSIONS

The present work includes the fabrication of a portable device for VOC detection with a transparent heater. A synthesis of black SnO_2 by a simple colloidal precipitation method is carried out. A pellet of black SnO_2 and S-IDE were fabricated

https://doi.org/10.1021/acsomega.1c03399
ACS Omega 2021, 6, 22900−22908

and used for analyzing the VOCs. At 315 K, the black SnO_2 pellet shows a 2 order increment in the current level under ethanol vapor exposure. At room temperature, S-IDE records a noticeable change in current for ethanol, IPA, and acetone. Also, the divergence of current for acetone vapors with different temperatures is examined. In all of the measurements, a positive shift of the Dirac point is observed. The Fermi level shift is observed with the shift in the Dirac point. Finally, the developed bottle setup is feasible and can be used in all research laboratories for primary VOC verification.

EXPERIMENTAL SECTION

The glass bottle is procured from Borosil, India. The chemicals ethanol (C_2H_5OH), isopropyl alcohol (C_3H_8O), acetone (C_3H_6O), and stannous chloride ($SnCl_2{\cdot}2H_2O$) are purchased from Thermo Fisher Scientific, USA; sodium hydroxide (NaOH) is procured from Nice Chemicals, India; and EA is procured from Sigma-Aldrich, Germany. All of the chemicals are used as received without any further purification. Grade 42 Whatman filter paper is procured from Whatman, USA; 8B pencil is purchased from Artline, Japan. The commercially available general-purpose printed circuit board is procured from the local market. Epoxy adhesive is procured from the local market. For all of the cleaning and sterilizing processes, deionized water (specific resistance, 18.2 MΩ cm) is used. Silver paste is purchased from Siltech Corporation, India. Double-sided supersticky tape is procured from 3M, USA. Commercially available transparent heaters were procured from North East Flex Heaters, USA. The masses of precursors and active materials are measured by a Shimadzu AX200 microbalance.

Design of the Portable Device. The design of a portable bottle setup is shown in Figure 15a. The backbone stick is made to run through the groove in the bottle cap. The backbone stick has two pairs of connecting wires. One pair of wires is used for microheaters, and another pair is used for a sensor to retrieve the data. The sensor is positioned at the end of the backbone. The indium tin oxide transparent microheater reaches a temperature of up to 150 °C with a variable DC power supply. The glass slide substrate of a microheater provides a plane surface for sensor mounting and uniform distribution of thermal energy to the sensor. Two terminals of a sensor are connected to the source meter. The transverse section of the sensing area is shown in Figure 15b.

For the functional verification of device setup, black SnO_2 pellet and black SnO_2/EA composites deposited on cellulose and pencil-based IDE are used to detect the VOCs.

Preparation of the Black SnO_2 Pellet. $SnCl_2{\cdot}2H_2O$ (0.153 M) is sonicated for 20 min; then, 0.5 g of NaOH is added to the $SnCl_2$ solution and stirred for 5 min. The solution turns into a white precipitated solution; then, 1 g of NaOH is added to the white precipitated solution and stirred for another 5 min until the solution turns into a black precipitated solution. The solution is stirred for another 30 min. The final solution is washed with DI water until a neutral pH is achieved. The black SnO_2 powder is collected and dried under a table lamp for 12 h. The obtained powder is used to make pellets using a hydraulic press at 40 psi, and it is shown in Figure S3.

Characterization. The surface morphology of black SnO_2 is understood by a scanning electron microscope (SEM) (JS-6360, JEOL, Japan) with EDX. The FTIR spectrum is recorded on a PerkinElmer Frontier MIR/FIR spectrometer, USA, in the form of black SnO_2 in a KBr pellet. UV/visible spectra are recorded on a UV/visible 1392 LABINDIA, India, with 190−900 nm scan. The crystal size is calculated by X-ray diffraction (XRD) data carried out on a D8 Advance, Bruker, Germany, equipped with Cu Kα radiation at a scan rate of 2°/min in the 10°−70° range. The current−voltage (I−V) measurements are carried out by a Keithley 2450 EC workstation equipped with a computer-controlled LabView program.

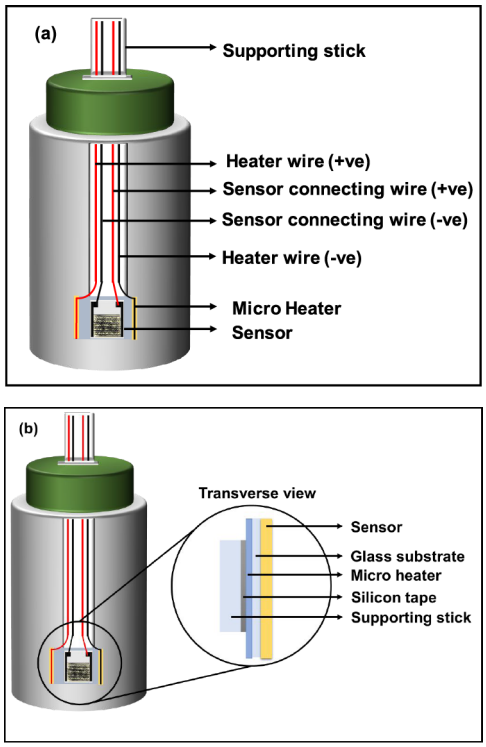

Figure 15. (a) Schematic design of the portable VOC sensing device setup and (b) transverse view design of the portable VOC sensing device.

Preparation of Black SnO_2, Egg Albumin Composite Deposited on Cellulose−Pencil-Based IDE. Grade 42 Whatman filter paper is used as a substrate, and 8B pencil is used to prepare interdigitated electrodes where bulk graphite acts as a current collector. EA (0.5 mg) is dissolved in 50 mL of DI water; three drops of the EA solution are poured on IDE and dried under a table lamp. Then, 0.153 M black SnO_2 is drop-cast on EA-deposited IDE and dried under the lamp for 2 h. The schematic representation of the preparation of black SnO_2 and EA composite deposited on cellulose−pencil-based IDE is shown in Figure 5.

Fabrication of the Microheater. Indium-doped tin oxide-coated glass slides cut into 1.5 × 1.3 cm^2, silver paste, and conducting copper tape are used to connect the copper leads to prepare the microheater for the device setup.

ASSOCIATED CONTENT

Supporting Information

The Supporting Information is available free of charge at https://pubs.acs.org/doi/10.1021/acsomega.1c03399.

UV−visible absorption spectrum (Figure S1); FTIR spectra of SnO_2 (Figure S2); and synthesized black SnO_2 used to prepare the pellet for the VOC measurements (Figure S3) (PDF)

https://doi.org/10.1021/acsomega.1c03399
ACS Omega 2021, 6, 22900−22908

AUTHOR INFORMATION

Corresponding Authors

Shridhar Mundinamani − *Department of Physics, Siddaganga Institute of Technology, Tumakuru, Karnataka 572103, India;* orcid.org/0000-0002-8048-0512; Email: mpshridhar@sit.ac.in

Gurumurthy Sangam Chandrasekhar − *Nanomaterials and Polymer Physics Lab, Department of Physics, Manipal Institute of Technology, Manipal Academy of Higher Education, Manipal, Karnataka 576104, India*; Email: gurumurthy.s.c@gmail.com

Authors

Kiran Mahalingappa − *Department of Electronics and Communication Engineering, Siddaganga Institute of Technology, Tumakuru, Karnataka 572103, India;* orcid.org/0000-0002-5714-8757

Gowtham Maralur Pranesh − *Department of Electronics and Communication Engineering, Siddaganga Institute of Technology, Tumakuru, Karnataka 572103, India*

Gopinatha Bidarkatte Manjunath − *Department of Electronics and Communication Engineering, Siddaganga Institute of Technology, Tumakuru, Karnataka 572103, India;* orcid.org/0000-0002-9337-4401

Shilpa Molakkalu Padre − *Nanomaterials and Polymer Physics Lab, Department of Physics, Manipal Institute of Technology, Manipal Academy of Higher Education, Manipal, Karnataka 576104, India*

Nirankar Nath Mishra − *Department of Nanotechnology, Siddaganga Institute of Technology, Tumakuru, Karnataka 572103, India*

Complete contact information is available at: https://pubs.acs.org/10.1021/acsomega.1c03399

Author Contributions

K.M., G.M.P., and G.B.M. performed all of the experiments; N.M. carried out the SEM and EDX measurements; G.S.C. performed S-IDE fabrication; and S.M. analyzed the data and wrote the manuscript. The authors have approved the final version of the manuscript.

Notes

The authors declare no competing financial interest.

ACKNOWLEDGMENTS

The author S.M. thanks VGST, Govt. of Karnataka, for the financial support under the SMYSR Programme (ref. letter no. No/VGST/GRD-585/2016-17/2017-18/39 dated April 19, 2018) and Siddaganga Institute of Technology, Tumakuru, for the financial support to procure instruments and chemicals. N.M. thanks Karnataka Council for Technological Upgradation, Govt. of Karnataka (KCTU/R&D/SIT-Nano/2016-17/399).

REFERENCES

(1) Srivastava, A. K. Detection of volatile organic compounds (VOCs) using SnO_2 gas-sensor array and artificial neural network. *Sens. Actuators, B* **2003**, *96*, 24−27.

(2) Tomer, V. K.; Duhan, S. Ordered mesoporous Ag-doped TiO_2/SnO_2 nanocomposite based highly sensitive and selective VOC sensors. *J. Mater. Chem. A* **2016**, *4*, 1033−1043.

(3) Kwok, N.-H.; Lee, S.-C.; Guo, H.; Hung, W.-T. Substrate effects on VOC emissions from an interior & finishing varnish. *Build. Environ.* **2003**, *38*, 1019−1026.

(4) Qin, X.; Wu, T.; Zhu, Y.; Shan, X.; Liu, C.; Tao, N. A Paper-Based Milli-Cantilever Sensor for Detecting Hydrocarbon Gases via Smartphone Camera. *Anal. Chem.* **2020**, *92*, 8480−8486.

(5) Martinez-Hipatl, C.; Munoz-Aguirre, S.; Munoz-Guerrero, R.; Castillo-Mixcoatl, J.; Beltran-Perez, G.; Gutierrez-Salgado, J. M. Optical system based on a CCD camera for ethanol detection. *Meas. Sci. Technol.* **2013**, *24*, No. 105003.

(6) Öztürk, S.; Kösemen, A.; Kösemen, Z. A.; Kılınç, N.; Öztürk, Z. Z.; Penza, M. Electrochemically growth of Pd doped ZnO nanorods on QCM for room temperature VOC sensors. *Sens. Actuators, B* **2016**, *222*, 280−289.

(7) Pargoletti, E.; Hossain, U. H.; Di Bernardo, I.; Chen, H.; Tran-Phu, T.; Lipton-Duffin, J.; Cappelletti, G.; Tricoli, A. Room-temperature photodetectors and VOC sensors based on graphene oxide−ZnO nano heterojunctions. *Nanoscale* **2019**, *11*, 22932−22945.

(8) Nguyen, H.; El-Safty, S. A. Meso- and Macroporous Co_3O_4 Nanorods for Effective VOC Gas Sensors. *J. Phys. Chem. C* **2011**, *115*, 8466−8474.

(9) Kashyap, A. K.; Kiran, M.; Devaraj, B. N.; Karthik, S. Review on Data Acquisition and Processing on E-nose. *IEEE Conference on Innovative Mechanisms for Industry Applications*, Bangalore, India, 2020. DOI: 10.1109/ICIMIA48430.2020.9074908

(10) Gopinatha, B. M.; Kiran, M.; Gowtham, M. P.; Mundinamani, S. P. Cellulose paper and Pencil based Smart Switch. *IEEE Conference on Smart Electronics and Communication*, Trichy, India, 2020. DOI: 10.1109/ICOSEC49089.2020.9215427

(11) Krzywiecki, M.; Grządziel, L.; Sarfraz, A.; Erbe, A. Charge transfer quantification in a SnOx/CuPc semiconductor heterostructure: Investigation of buried interface energy structure by photoelectron spectroscopies. *Phys. Chem. Chem. Phys.* **2017**, *19*, 11816−11824.

(12) Churkina, G.; Kuik, F.; Bonn, B.; Lauer, A.; Grote, R.; Tomiak, K.; Butler, T. M. Effect of VOC Emissions from Vegetation on Air Quality in Berlin during a Heatwave. *Environ. Sci. Technol.* **2017**, *51*, 6120−6130.

(13) Jang, A.-R.; Jeon, E. K.; Kang, D.; Kim, G.; Kim, B.-S.; Kang, D. J.; Shin, H. S. Reversibly Light-Modulated Dirac Point of Graphene Functionalized with Spiropyran. *ACS Nano* **2012**, *6*, 9207−9213.